Sol-gel TiO 2 nanoimprinted metasurface combined to hybrid-silica sensitive layers for selective VOC detection with high refractive index sensitivity

Mehrnaz Modaresialam, Gabrielle Bordelet, Zeinab Chehadi, Martin O'Byrnen, Luc Favre, Magali Putero, Marco Abbarchi, David Grosso

Sol-gel TiO_2 nanoimprinted metasurface combined to hybrid-silica sensitive layers for selective VOC detection with high refractive index sensitivity.

*Mehrnaz Modaresialam,[1] Gabrielle Bordelet,[1] Zeinab Chehadi,[1] Martin O'Byrnen,[1] Luc Favre,[1] Magali Putero,[1] Marco Abbarchi,[1] David Grosso.[1]**

[1] Aix Marseille Université, Université de Toulon, CNRS, IM2NP, UMR 7334, Campus de St. Jérôme, 13397 Marseille, France.

TOC

VOC detection at sub-ppm levels, associated to a high RI variation sensitivity, was achieved by direct reflection on a surface composed of sol-gel organic-inorganic microporous sensitive layers embedding an array of 140 nm TiO_2 pillar antennas prepared by sol-gel nanoimprint. Such a performance was attributed to the electromagnetic confinement within the Titania pillars, enhancing the interaction of the radiation with the sensitive media. The system also shows a relatively good selectivity by comparing the adsorption of five different VOCs with various polarity indexes within six different sensitive sol-gel layers.

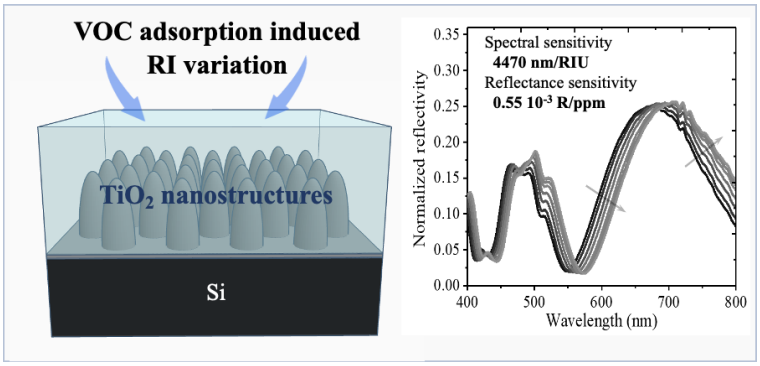

Abstract

We combine all-dielectric, metal oxides, sensitive materials based on sol-gel deposition with metasurfaces formed via Nano Imprint Lithography, to form nanocomposite systems with high sensitivity for refractive index (RI) variations and volatile organic compounds (VOC) concentrations in air. We show spectral shifts of 4470 nm / RIU and 0.2 nm / ppm and reflection intensity changes of R^* = 17 and 0.55 10^{-3} R / ppm. The metasurface is composed of TiO_2 high aspect ratio nano pillars array, whereas the surrounding sensitive materials are class *II* hybrid silica microporous materials embedding various types of covalently bonded organic functions. These hybrid layers showed marked relative differences in chemical affinity with different VOCs that are

exploited to detect them and eliminate interferences with air moisture for qualitative analysis of gas mixtures. The presence of the TiO_2 metasurface enhances the signal by almost an order of magnitude with respect to the 2D counterpart and is attributed to the antenna effect, enhancing the interaction of the confined electromagnetic wave with the sensitive medium. This sol-gel nanocomposite system presents many advantages such as high throughput and low-cost elaboration of the elements, and a high chemical mechanical and thermal stability, ensuring a high stability for detection for long periods of time.

1. Introduction

Refractive Index (RI) sensitive materials are critical elements for environmental analysis through optical transduction in chemical, biological, and physical sensors. They rely on variations of electromagnetic confinement in metals (Localized Surface Plasmonic Resonances, LSPR) or dielectrics (Fabry-Perot interferences, Mie resonances) upon small changes of RI in the confinement volume of the electromagnetic waves. [1],[2] Size and geometry of micro- and nano-structures are thus designed to enhance the electromagnetic resonances in the regions where the RI changes. In chemical sensing, such a variation is induced at the surface or inside the material (if porous) through the modification of the chemical environment triggered by combination of a target molecule with a specific host chemical group or simply by adsorption. [3] Gas sensing is a category of detector that suffers from a high competitivity of adsorption between the molecules composing the air. For instance, Volatile Organic Compounds (VOC) are more or less toxic molecules produced by different human activities or nature. There are many of them and they cohabit in the air at low concentrations (*e.g.* ppm levels) [4] with water that is the most critical interferent due to its high concentration. These small molecules tend to interact easily with surfaces, rendering them easy to quantify as this phenomenon is governed by thermodynamic equilibrium. However, designing a sensor that is selective to one VOC is extremely challenging. [4]

Chemical sensors based on optical transduction through RI variations rely on measuring either wavelength shifts or intensity variations (Reflectance R, Transmittance T, or Scattering S). Many different metasurfaces or metamaterials have been designed and studied to enhance the optical signal and increase the performance. Sensitivity *S* ($S = \Delta\lambda/\Delta n$ and Figure of Merit *FOM* ($FOM = S/FWHM$ with *FWHM* being the Full Width at Half Maximum of the resonance) are indicators of performance considering both resonance sharpness and wavelength shift upon RI change. Alternatively, detection can be based on R, S or T intensity variation that are usually compared through the "alternative" Figure of Merit *R** $\left(R = (\Delta I/I)/\Delta n\right)$ given as *R, S or T / RIU*. Due to their relatively sharp LSPR and narrow wavelength-shift, gold or silver nanostructures (core-shell) nanoparticles [5], pillars [6], disks [7], rods [8], pyramids [9], stars, etc., are the most attractive metasurfaces for RI sensing: sensitivity up to 2.10^3 nm / RIU (Refractive Index Unit), with a *FOM* of 100 [6], have been experimentally evidenced with gold nanopillars, while simulations with gold nano shell systems revealed a potential sensitivity of 3.10^3 with a *FOM* around 10[10].

More recently, dielectric (Si, Ge, Metal oxides (MO_n)) nanostructures have been considered as alternative RI sensitive materials due to their low toxicity, low cost and fabrication easiness. Interestingly, the possibility to select the intrinsic RI of some dielectrics, such as MO_n, enables optimizing sensing within specific RI spans. The electromagnetic confinement in dielectric nano objects leads to a strong modifications of R, T and S intensity and can be highly sensitive to the

surrounding RI [2], [11]. First examples concerned combined dielectrics and metals [12,13] in complex architectures. For instance, *FOM* values up 6.7 x 10^3 are deduced from simulations with Au/SiO_2-Al_2O_3 pillar systems. [14] Finally, Al/Al_2O_3 ring systems provided an experimental *FOM* of 6 for Δn = 0.6. [13] For pure dielectric systems, a *R** of 6 was experimentally demonstrated for SiGeTe nano spheres [11], whereas the highest value simulated for metal oxide (*e.g.*, V_2O_5, TiO_2) patterns reaches 13 [15]. The following Table 1 reports state-of-the-art *FOM*, *R**, Q-factors and sensitivity for these classes of materials.[16–20] It reveals that high performances are achieved with complex metals or semiconductor (SC) architectures, while the more attractive ones have only being modelled without experimental corroborations.

Table 1. Comparison of state-of-the-art sensitivities, FOM, R and Q factor of different refractive index-based sensors from the literature with those reported in this current work (Exp. and Sim. stand for experimental and simulated values, respectively).*

Materials	*S* nm/RIU	*FOM*	*S*,*T*,*R* / RIU	*Q*-factor	References
Metals (Au, Al)	Exp : up to 10^3 *Sim. : up to 3.10^3*	Exp: 10 to 110 -	- -	- -	[1,6,7,10,12,21,22]
SC (Si, Ge, Te)	Exp : 200 to 920 *Sim. : 350 to 2.10^3*	Exp: 2 to 120 *Sim. : 80 to 2.10^3*	Exp : 4 to 9 -	Exp : up to 10^3 *Sim. :up to 10^5*	[2,11,16,18,19,23]
Metal/MO_n	Exp : up to 10^3 *Sim. : up to 2.10^3*	Exp : 6 *Sim. : 500 to 6.10^3*	- -	Exp : 26-27 -	[14,22,25]
MO_n (V_2O_5, TiO_2)	*Sim. : 10 to 800*	*Sim. : 732*	*Sim. : 13*	-	[15,24]
TiO_2	***Exp : 4500***	***Exp : 12***	***Exp : 17***	***Exp : 4***	***This work***

Detecting gas by optical transduction often requires a porous sensitive material with inner pore surface being covered with a chemical group that has a good affinity with the target molecules. These materials need to be highly porous, with a high specific surface area (micro- or meso-pores with high accessibility), robust and stable, easy to process as optical elements. [26–28] Among them, sol-gel based materials gather these features providing an excellent versatility to tune porosity, chemical composition and RI as thin coatings[29].

Silica-based layers have been exploited in this work as sensitive materials with refractive index around RI_0 ~ 1.5. Since VOC need to be detected at ppm levels (0 to 100 ppm) through adsorption, the porosity needs to be adapted so that the sensitivity is maximal, and ideally with a linear dependence on concentration, for extremely small RI increases from RI_0 of the desorbed material. As such, microporous materials with pore dimension < 2 nm are ideal since they exhibit a high specific surface area (high density of adsorption sites) enabling high adsorption at low relative vapor pressures (P/P_0). Such pores can be further chemically adapted to tune the adsorption affinity with specific types of VOC molecules exhibiting different polarity index. Owing to the small size of VOC, forbidding an individual molecular identification, it is thus only possible to modulate the chemical affinity during adsorption by changing the polarity of the pore surface with organic functions that exhibit more or less polar characteristics.

Such materials are elaborated as thin films using simple high throughput chemical liquid deposition processes such as dip-coating [30]. They require further thermal curing, typically around 400°C to stabilize the inorganic backbone, but this treatment should be adapted to prevent decomposition of

Code de champ modifié
Code de champ modifié
Code de champ modifié
Code de champ modifié

the organic function. Since such materials are never sensitive to a single VOC molecule and are also relatively insensitive to humidity, one may combine several of them in a single "artificial nose" device to provide several signals that would be analyzed using Machine-Learning technology.

Mis en forme : Anglais (États-Unis)

The aim of this work is to demonstrate that the combination of all-dielectric metal oxides sensitive materials and metasurfaces, all prepared by simple high throughput sol-gel methods, can lead to relatively high sensitivity (1 ppm) and relatively good chemical selectivity for VOC sensing, using simple reflectivity transduction at visible frequency. First, several microporous hybrid silica (H-SiO_2) layers have been elaborated with different organic contents and tested as adsorbents with common VOC, such as isopropanol, acetone, chloroform, hexane, toluene and water as adsorbates. 1 ppm of adsorbate in air can increase the layer RI by 10^{-4}. Besides, adsorbent/adsorbate pairs showed relatively different affinities one to the other, which could be exploited in artificial noses to address the chemical selectivity. One of these pairs has then been selected and combined with a TiO_2 metasurface to prepare a nanostructured composite sensitive layer. The metasurface is composed of TiO_2 (Anatase) nano-pillars, and is obtained by Nano Imprint Lithography [31–33] and organized in a 2D hexagonal pattern on a Si wafer. It is then capped by the microporous Hybrid silica (H-SiO_2) layer. The reflectivity of the layer has then been measured in the visible range with increasing vapor pressure. The measured sensing performances are: sensitivity *S* up to 4500 nm / RIU, reflectivity variation up to 15 R / RIU, *FOM* up to 12, with a Q-Factor of 4 for specific wavelength, which is compatible with sub-ppm gas detection by simple specular reflection. These performances have been compared to the theoretical responses of the corresponding Bruggeman Effective Medium Approximation (BEMA) model of the system, revealing the critical role of the pillar in exalting the signal. Structural characterizations and spectroscopy were performed by FTIR, HR-SEM, TEM, AFM, XRD, and ellipsometry.

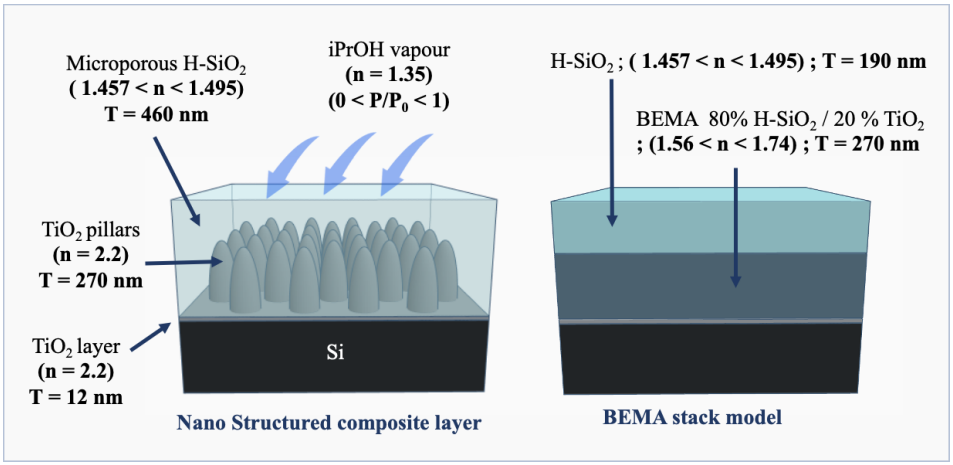

Figure 1. Scheme representing the experimental nanostructured composite system (experimental) and the corresponding Bruggeman Effective Medium Approximation BEMA multilayer stack system (model) used as sensitive coatings for RI variation and VOC concentration detection. The variation of RI is induced by the controlled adsorption of isopropanol into the H-SiO_2 material (layer).

2. Experimental section

Preparation of hybrid-silica sensitive plain coatings

All chemicals were purchased from Aldrich. In a typical procedure, TetraEthylOrthoSilicate (TEOS) and hybrid silanes precursors were dissolved in a mixture of 25 isopropanol: 11 water: 3 hydrochloric acid (molar ratio), with molar ratios of precursors provided in table 2. Solutions were aged 1 day at room temperature before using for film deposition (shelf-life between 2 and 10 weeks).

Table 2. Molar ratios of the chemical solutions precursor

Solutions	Silane precursors (molar ratio Precursor / Si)
REF	1 Tetraethoxysilane (S)
S3M3P3	0.3 (S) 0.33 Methyl triethoxysilane (M) 0.34 Phenyltriethoxysilane (P)
S4T6	0.4 (S) 0.6 p-Tolyltrimethoxysilane (T)
S3M3T4	0.3 (S) 0.3 (M) 0.4 (T)
S4M3Np3	0.4 (S) 0.3 (M) 0.3 1-Naphtyl tri-methoxysilane (NP)
S3M3PP3	0.3 (S) 0.3 (M) 0.3 4-bi-Phenylyl tri-ethoxysilane (PP)

Silicon wafer substrates were first cleaned with detergent, acetone and ethanol in a ultra-sound bath. Depositions were performed by dip-coating using an ACE-dip from Solgelway between 1 and 6 $mm.s^{-1}$ at low humidity (< 10%) to adjust the final thickness between 300 and 600 nm, depending on the solution viscosity. As-prepared coatings were then calcined at 400 °C for 10 min. Final refractive indices were between 1.42 and 1.57, depending on the film composition.

Preparation of Titanium dioxide plain film

Titania solution was prepared by mixing molar ratios of 1 $TiCl_4$; 40 EtOH; 7 H_2O; 2.10^{-5} F127 (Pluronics F127: PEO-PPO-PEO) all purchased from Aldrich. After 24 h aging at room temperature, the solution was dip coated on Si wafer at 2 $mm.s^{-1}$ withdrawal speed under relative humidity HR < 10%. The as-prepared film was either used directly for nanoimprint (see below) or calcined at 450 °C for 10 min under infrared lamps to yield a final thickness of 75 nm and a RI of n = 2.252 at 633 nm.

Preparation of S3M3P3/TiO_2 nanostructured composite coating.

A commercial perfluoropolyether Fluorolink (MD700) master was first replicated in Perfluoropolyether (PFPE) to obtained the inversed mold. To do so, a few droplets of PFPE precursors were applied on the center of the master and spread homogenously using a solid roller. The mold was peeled off from the master after 10 min of curing under nitrogen and ultra-violet LED (365 nm, 4 W). The mold was then degassed for 10 min in primary vacuum. As-prepared titania sol-gel films were directly transferred from the dip-coater into a nano imprint chamber in which a 22 °C temperature and a 50% relative humidity were maintained using a constant $5L.min^{-1}$ flux from a Solgelway humidity controller. The degassed PFPE mold was applied onto the sol-gel film and maintained at 60 °C for 15 min before demolding. The imprinted sol-gel patterns were

then annealed at 450 °C for 10 min to ensure complete removal of the F127 polymer and crystallization. The microporous organic-inorganic S3M3P3 silica layer was coated on top of the TiO_2 pattern by dip-coating at RT using 4 $mm.s^{-1}$. Then, the final nanostructured composite coating was annealed at 400 °C for 10 min for stiffening.

Structural and chemical analysis of the nanocomposite coating.

Structural investigation of the nanoimprinted samples was performed by atomic force microscopy (AFM, PSIA XE-100) and high-resolution scanning electron microscopy (HR-SEM) after Focused Ion Beam (FIB) milling (Dual-beam FIB FEI HELIOS 600 NanoLab). Focused Ion Beam etching was performed at 30 keV with Ga^+ ions. HR-SEM images were collected using secondary electrons with the in-lens detector at 5 keV. X-ray Diffraction (XRD) investigation was performed in order to check the crystalline phases of TiO_2 plain films and metasurfaces. XRD patterns were recorded on a conventional diffractometer (PANalytical Empyrean) using Cu radiation (λ = 0.154 nm), and a rapid detector (PANalytical PIXcel) in Bragg-Brentano geometry. Fourier Transform InfraRed spectroscopy (FTIR) spectra were collected in transmission mode directly on the sensitive layer deposited on Si wafers using a PerkinElmer (Sprectrum Two) spectrometer.

Spectroscopic investigations.

Thicknesses and refractive index of pure plain (non-imprinted) TiO_2 and S3M3P3 coatings were determined with a Spectroscopic Ellipsometry (Woollan M2000V) instrument and a Cauchy model for transparent materials. The variation of RI of the S3M3P3 sensitive coatings with respect to gas adsorption was followed *in situ* using an environmental chamber. The gas was selected to be iPrOH for its high volatility and its good affinity with the layer. Its relative pressure (P/P_0) was adjusted using an air-dilutor system, mixing both iPrOH saturated and pure airs. Normalized reflected intensity spectra on the nanostructure composite layer were collected at 45° incident angle, between 380 and 1000 nm for different values of P/P_0 ($1.45 < n_{S3M3P3} < 1.5$). The theoretical reflectivity of the Bruggeman Effective Medium Approximation (BEMA) model (see Figure 1), corresponding to the nanocomposite system, was generated from the CompleteEASE software of the ellipsometer using experimental structural data and 45° incident angle.

3. Results and discussion

Investigation of gas adsorption in plain sensitive layers.

First, plain layers of sensitive H-SiO_2 materials were tested in different VOC vapor environments at 0% humidity to avoid perturbation due to adsorbed water. The refractive index variations δn were measured using spectroscopic ellipsometry. Figure 2a) provides the adsorption isotherm of isopropanol in the S3M3P3 sensitive layer, confirming the typical Langmuir behavior for microporous materials, following equation (1) for which the fit parameters were found to be δ_{nmax} = 0.044 and the affinity constant b = 22. Using $P_{IPrOHsat}$ = 2 kPa, one can then deduce equation (2) that links the measured δ_n to the concentration in ppm of adsorbate in the environment. To detect 2 ppm of iPrOH in air at 1 Atm and 20 °C, one needs to be able to detect a $\delta_n = 10^{-4}$.

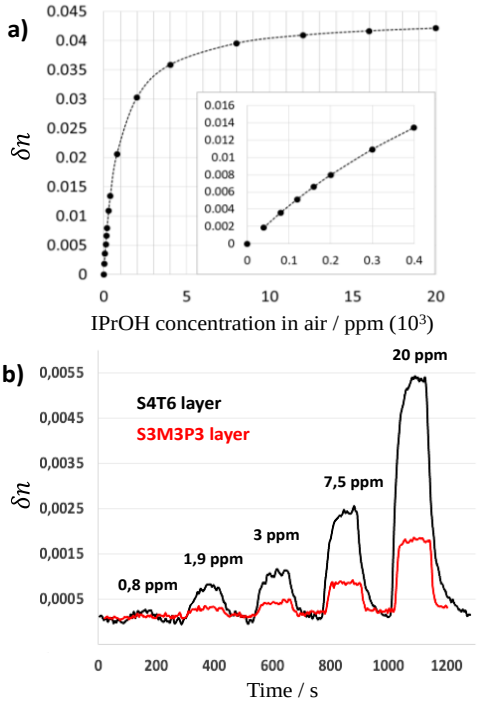

Figure 2. a) Adsorption isotherm of isopropanol in S3M3P3 sensitive plain layer, plotted as δ_n, measured by spectroscopic ellipsometry, vs. iPrOH concentration. b) Variation of refractive index of S4T6 and S3M3P3 plain layers, measured by ellipsometry through exposition to different concentrations of isopropanol in dry air.

$$\delta n = \delta n_{max} \frac{b\left(\frac{P}{P_0}\right)}{\left(1+b\left(\frac{P}{P_0}\right)\right)} \qquad \textbf{(1)}$$

$$C_{IPrOH} = \frac{10^6 P_{IPrOHsat} \delta n}{P_{Atm}(0{,}97-22\delta n)} \qquad \textbf{(2)}$$

Figure 2b) shows the evolution of δ_n measured by ellipsometry on a S4T6 and a S3M3P3 layers in presence of small concentrations of n-hexane at 0% humidity. One remarks first that $\delta_n = 10^{-4}$ is the resolution of the ellipsometer. It will be demonstrated in the second part of the article that sub-ppm detection is achievable with a much simpler method than ellipsometry. Both films do not show the same RI variation for the same concentration of vapor. Such significant differences in adsorbate/adsorbent chemical affinity is attributed to the different chemical composition and porosity of the two layers. The porosity of the films cannot be directly compared, but one can verify the presence of the introduced chemical functions from FTIR spectroscopy as in Figure 3A). It is clear that, even if calcined at 400 °C, the films still embed the methyl and the aromatic functions introduced as precursors. They should thus be accessible as adsorption sites to the VOC adsorbates through the porosity and must play a crucial role in the chemical affinity difference. To go further, when testing the SiO_2 reference (REF) and the five different H-SiO_2 layers with the five different VOCs at a concentration of 600 ppm, and with 100% humidity (saturation), one observes that each pair present a specific affinity that is due to the difference in the layer chemical and porosity characteristics and in the VOC index of polarity (see Figure 3B)).

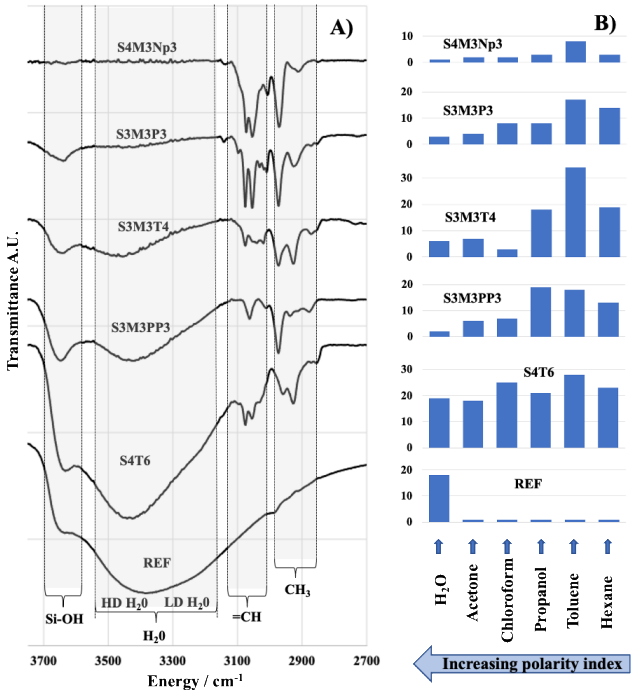

Figure 3. A) FTIR spectra of sensitive layer showing regions of C-H stretching from methyl and aromatic functions, and regions of O-H stretching from water (High Density (liq.); Low Density (sol.)), and silanol. B) Comparison of chemical affinity measured on a set of sensitive layer adsorbent / VOC adsorbate pairs when submitted to 600 ppm of VOC or to 100% humidity ($10^3\ \delta_n$).

As expected, the REF layer mainly adsorbs water since it contains no organics, but only highly polar Si-OH groups on the pore walls. Such reference layer acts thus as a water-selective sensitive layer, that is used to assess humidity between 0 and 100% and to correct the water up-take into the other hydrophobic layers. Indeed, the other H-SiO_2 layers are more prone to interact with VOCs, since their adsorption of water at 100% RH is much lower than the adsorption of VOCs at 600ppm. This suggests that the less polar methyl and unsaturated phenyl, bi-phenyl, tolyl and naphthyl groups are pendent and occupy most accessible adsorption sites at the pore wall surface. It has been demonstrated that when methyl groups are attached to a Si-O-Si backbone, they tend to position at the interface with the pore nanocavities upon thermal annealing without decomposing due to the stability of the Si-C bond below 450 °C in air [34]. The same behavior is verified for the unsaturated rings by FTIR investigations.

Since all H-SiO_2 layers do not adsorb water with the same affinity, it occurs that porosity and distribution of polar OH and less-polar P, T, M, PP, Np groups are different for each layer, certainly due to the influence of the organics on the condensation of the silica network during solution ageing, film drying, and thermal treatment. S4T6 layer adsorbs water and the five VOCs with relatively similar affinity. It thus acts as a "universal" adsorber in the present work. The four remaining H-SiO_2 shows relative different affinities with the VOC and will serve for differencing adsorbates (VOC with low polarity index being favorably adsorbed when high concentration of hydrophobic functions are present). However, to do so, competitive adsorptions of VOCs in H-SiO_2 layer must be as low as possible, especially with water. When two of the selected vapors are injected in the chamber at the same time, such as for example iPrOH and water, they must not interfere, at least at low pressures. This has been confirmed in Figure 4 that shows the evolution of δ_n in the S3M3P3 layer when submitted successively to 100, 220, and 350 ppm of isopropanol, together with 0, 30, 60 and 90% of relative humidity.

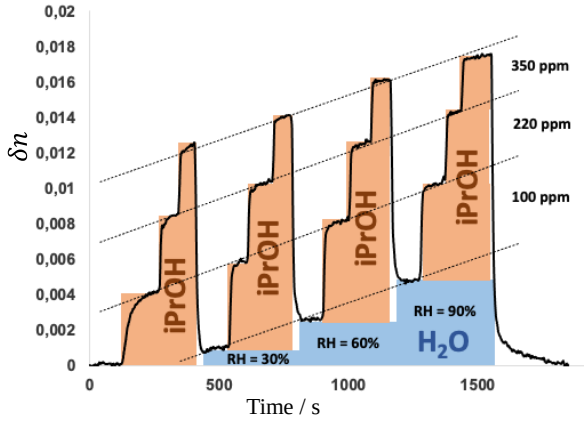

Figure 4. Variation of δ_n measured by ellipsometry on the S3M3P3 plain sensitive layer when submitted to 100, 220 and 350 ppm of isopropanol and 0, 30, 60, and 90 % humidity.

It is clear from the results that whatever the relative humidity, the RI increasing for a given VOC concentration is constant, and add to the δ_n induced by the water uptake. One may carefully mention at this stage that adsorption sites are relatively specific in such H-SiO_2 microporous materials. These results confirm that they are partially selective to specific types of vapors, and can be combined together into an optical sensor to design an artificial nose. A dip study of selectivity in such materials is somewhat extremely interesting but is out of the scope of the paper, that will concentrate in the following second part on sensitivity enhancement.

Performances of nanostructured sensitive layer assessed in direct specular reflection

While ellipsometry has been used in the previous part to assess RI variations, the following par will focus on a simpler method based on specular reflectivity to asses VOC concentration in atmosphere. To do so, only one adsorbate/adsorbent pair will be used to investigate performances in sensitivity, since the transduction exploits RI variations. The S3M3P3/isopropanol pair has been selected as representative of all other possible pairs (see Figure 3). Experiments were conducted on a sensitive coating composed of a high index TiO_2 metasurface, elaborated on Si wafer and embedded into a layer of the S3M3P3 material. The role of the metasurface is to confine the visible electromagnetic radiations inside the high index nanofeatures to enhance their interaction with the surrounding sensitive material. The incident and collection angles were fixed at 45° as this configuration provided a good penetration of the mixed SP polarized light into the nanostructure coating (Brewster angle ≈ 55°), while collecting high enough reflected intensity. To assess the effective influence of the metasurface, the experimental reflectance was then compared to the simulated reflectance of a corresponding 3 layers stack coating for which the nanostructured composite thickness of the experimental sample was replaced by a Bruggeman Effective Medium Approximation layer (see Figure 1).

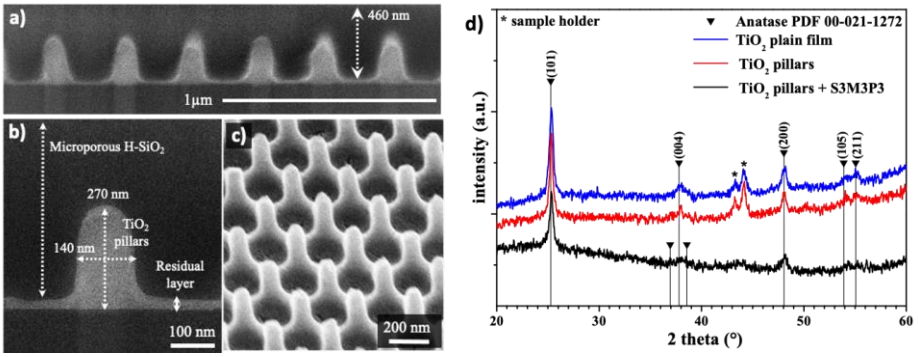

Figure 5. SEM images of a) and b) H-SiO_2-S3M3P3 / TiO_2 nanostructured composite, and c) of TiO_2 nanostructured metasurface. d) XRD patterns of the TiO_2 plain layer, the array of TiO_2 pillars, and the H-SiO_2-S3M3P3 / TiO_2 nanostructured composite.

Figure 5a-c) shows the SEM images of the nanostructured composite coating, revealing the array of TiO_2 pillars homogeneously organized in a 2D hexagonal pattern. The pillar aspect ratio is ~ 2

with 270 nm height and 140 nm width. A residual layer of about 10 to 20 nm thickness was spotted all over the Si wafer. After applying the S3M3P3 layer, the interpillar voids were totally filled up with the sensitive microporous material, while a plain layer of 190 nm thick extends above of the pillars. XRD investigations (Figure 5 d)) reveals that TiO_2 plain layer and pillar array were composed of Tetragonal Anatase (see PDF) Titania with the characteristic 101, 004, 200, 105 and 211 diffraction peaks of poly-oriented crystal. Both diagrams show very similar peak features, peak width (FWHM) and intensity, suggesting that the nanoimprinting does not change significantly the overall structuration induced by the thermal annealing. Fitting the diffraction peaks allows to deduce FWHM which is inversely related to the crystal size (along the direction of the scattering vector i.e. the direction normal to the film, and neglecting microstrain contributions). Using the Scherrer formula reveals nanocrystals of 16±1 nm for the plain layer and 18±4nm for the pillars. This is an important statement since the refractive index of the pillars, used in the BEMA model (see below), is extracted from the ellipsometry analysis of the plain layer. The fact that the Anatase crystals have similar average dimension around 20 nm suggests that RI are significantly close in both geometries.

A simple geometrical calculation based on the pillar dimensions and distribution (assuming a cylindrical shape) provides a composite thickness of 20% Vol TiO_2 and 80% Vol S3M3P3. The roughness of the top S3M3P3 layer was about 0.8 nm (RMS) from AFM analysis (not shown). Refractive indices of TiO_2 and S3M3P3 materials measured by ellipsometry on plain layers are 2.252 and 1.457 at 633 nm in dry air, respectively.

As studied in the first part, the refractive index of the sensitive layer increases with vapor pressure of isopropanol being introduced into the chamber, following a classical adsorption/desorption equilibrium behavior in microporous materials (Figure 2a). The vapor up-take is very large at low-pressure, going from 1.4570 to 1.4696 ± 10^{-4} (RI) between $P/P_0 = 0$ and 0.02. In the following investigations, only this range will be explored since for gas detection, sensitivity at low concentrations must be as high as possible (*i.e.* $P/P_0 = 0.02$ corresponds to 850 ppm in iPrOH at 20°C). The variation of Titania refractive index for the same vapor pressure is insignificant. As for pure Titania system, the RI of the sensitive material in the nanostructured composite system cannot be measured and is thus assumed to be that one of the plain layer counterpart.

Specular reflectivity spectra for the nanostructured composite system between $P/P_0 = 0$ and $P/P_0 = 0.02$ ($n_{S3M3P3} = 1.4570$ and 1.4696, respectively) are plotted in Figure 6a). These are compared to the simulated reflection spectra of the corresponding theoretical BEMA system calculated for the same δ_n increments, in Figure 6b). Both show a typical etalon interference trend that are relatively similar, especially at long wavelength. The lower intensity of the experimental signal at short wavelength (see Figure 6c)) is likely due to scattering effect of the pillars, this effect being attenuated at lower energy.

While the BEMA spectra undergo a global red shift of 6 nm around 670 nm, attributed to the S3M3P3 RI increase of 0.0126, a red shift of around 60 nm for the same interference is observed for the nanostructured system for the same δ_n increment. The corresponding Q-factor is 4 at (λ_{max} = 675 nm) for both systems. This difference is attributed to the TiO_2 metasurface antenna effect. Figure 6d) shows the plot of the wavelength of the interference maxima versus RI for the

nanostructured system. A linear RI sensitivity of around 4500 nm / RIU is found up to RI = 1.463, which is extremely high and corresponds to a sensitivity of 0.2 nm/ppm of iPrOH vapor in the atmosphere. The corresponding *FOM* = 12. Such a good sensitivity corresponds to the S3M3P3/iPrOH pair. Higher sensitivity should be found for pairs with higher chemical affinity.

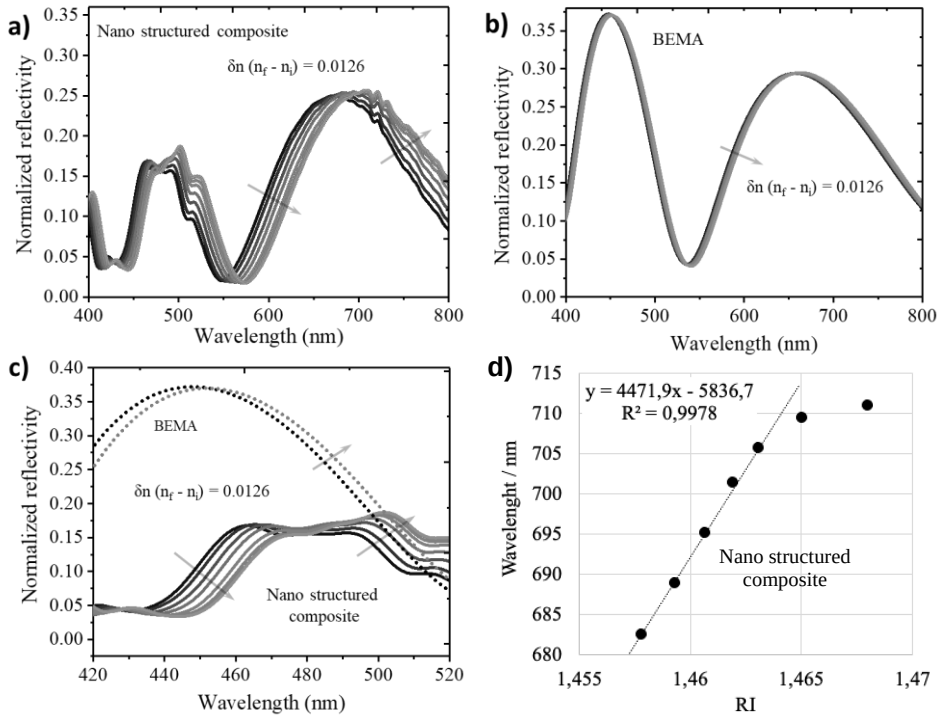

Figure 6. Reflectivity spectra measured at 45° incidence for the S3M3P3/TiO_2 nanostructured composite, a) and c), and simulated for the corresponding BEMA model, b) and c), for different increments of δ_n between 1.4570 and 1.4696. d) λ_{max} vs. RI (sensitivity) extracted from a).

Using optical transduction through spectral shift requires spectral analysis of the signal. More conveniently, RI variation detection can also be performed at a single wavelength using the reflected intensity collected by a photodiode.[35] In such ultimate simplified methods, the sensitivity if provided by the R^* (equation (3)) for a given wavelength, and for a given RI span.

$$R_{(\lambda,n_i,\delta n)} = \frac{\left(R_{\lambda,(n_i+\delta n)} - R_{\lambda,n_i}\right)}{\delta n} \quad (3)$$

The dispersion of R^* has been determined for both the experimental and simulated reflectivity variation for different incremental δn and for different initial RI comprised between 1.4570 and

1.4665, which corresponds to the iPrOH concentration range 0 – 250 ppm. Figure 7 provides different plots of the results.

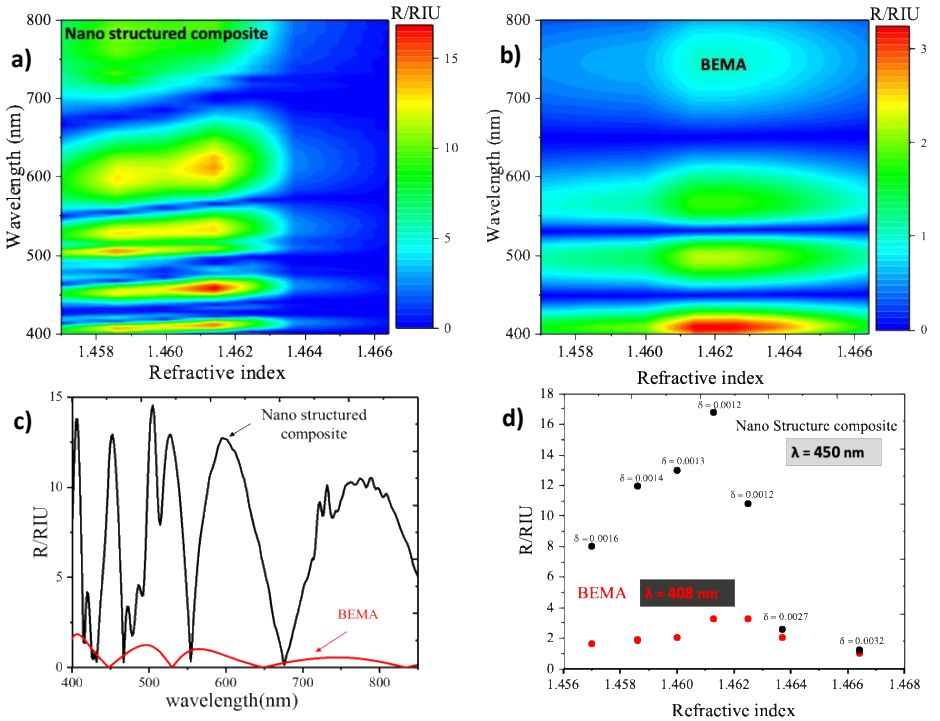

Figure 7. a) and b) 2D mapping of R dispersion values for different RI measured for the S3M3P3/TiO_2 nanostructured composite system and simulated for the BEMA system, respectively. c) and d) R* dispersion and values extracted from a) and b) for both systems at an optimal wavelength of 450 and 408 nm.*

For the BEMA model, for which the Nano-structuration of the TiO_2/S3M3P3 composite layer is not considered, *R** has maximal absolute values between 1.5 and 3, resulting from the local reflected intensity variation induced by the red shift of the interference fringes. In the same conditions, the nanocomposite *R** can achieve absolute values from 8 to 17, which is almost one order of magnitude higher than the *R** of the BEMA model. These mapping clearly reveals that the *R** can take values with drastic differences depending on the wavelength, but also on the initial RI (n_i). Thus, in order to maximize the response, we select a wavelength of 408 nm for the BEMA model, and at 450 nm for the nanostructured system (in principle, narrow band illumination at about 450 nm can be provided with blue LEDs).

We now compare the maximal reflectance sensitivity provided in Figure 7a). The highest *R** = 17 / RIU is found at 450 nm for n_i = 1.4607 and n_f = 1.4619. It drops to 8 between n_i = 1.4562 and n_f = 1.4578. For these two conditions the sensitivity corresponds to a 0.36 10^{-3} R / ppm between 0 and

35 ppm and 0.55 10^{-3} R / ppm between 98 and 135 ppm. This suggests that if the analysis is to be performed at a specific wavelength such as 450 nm of a blue LED, the variation of R^* has to be implemented in the signal treatment for the whole RI detection span through a careful calibration.

4. Conclusion

We reported that the presence of a dielectric metasurface (TiO_2 pillar arrays) can significantly increase the sensitivity to RI variations in the surrounding medium in direct reflection up to 4500 nm / RIU. However, such high sensitivity can only be found in narrow conditions including wavelength, incident angle, RI and RI span. The metasurface has also been combined with microporous sol-gel layers to detect VOC by adsorption. Optimal sub-ppm sensitivity of 0.2 nm/ppm (spectral shift) and 0.55 10^{-3} R / ppm (single wavelength reflectivity) were demonstrated. Even if Q-factor and *FOM* were relatively low, the sensitivities were sensibly higher than those reported for plasmon-based system and those simulated for pure metal oxide metasurfaces (see Table 1). We also showed that robust and stable silica-based hybrid layers composed of different pendent organic moieties on the inorganic backbone have different chemical affinity with different VOC. The combination of a TiO_2 metasurface and sol-gel sensitive materials provide a good sensitivity and selectivity that constitutes critical transduction elements to design and elaborate a cost-effective "artificial nose" for VOC sensing. The present performances could be further increased through designing a more appropriated metasurface.

Acknowledgements

This material is based on the work supported in part by the National Science Foundation under the International Research Fellowship Program (grant OISE-0505786). The authors also acknowledge funding provided by CNRS ,UPMC and IUF (Institut Universitaire de France) , the PRCI network ULYSSES (no. ANR-15-CE24-0027-01) funded by the French ANR agency, the A*MIDEX foundation (ANR-11-IDEX-0001-02), the A*MIDEX project TITANIDE (no. A-M-AAP-EI-17-58-170228-16.21-ABBARCHI-SAT), and the FET-OPEN project NARCISO (no. 828890). We acknowledge the facilities of the NANOTECMAT platform at the IM2NP Institute.

Abbreviation

RI Refractive Index

VOC Volatile Organic Compounds

LSPR Localized Surface Plasmonic Resonances

FOM Figure Of Merit

BEMA Bruggeman Effective Medium Approximation

FTIR Fourier Transform InfraRed spectroscopy

HR-SEM High Resolution Scanning Electron Microscopy

TEM Transmission Electron Microscopy

AFM Atomic Force Microscopy

XRD X-Ray Diffraction

RMS Roughness Mean Square

References

[1] J. Becker, A. Trügler, A. Jakab, U. Hohenester, C. Sönnichsen, *Plasmonics* **2010**, *5*, 161.

[2] J. Yan, P. Liu, Z. Lin, G. Yang, *Nanoscale* **2016**, *8*, 5996.

[3] Y. Jian, W. Hu, Z. Zhao, P. Cheng, H. Haick, M. Yao, W. Wu, *Nano-Micro Lett.* **2020**, *12*, 71.

[4] B. Szulczyński, J. Gębicki, *Environments* **2017**, *4*, 21.

[5] Y. Sun, Y. Xia, *Anal. Chem.* **2002**, *74*, 5297.

[6] Y. Shen, J. Zhou, T. Liu, Y. Tao, R. Jiang, M. Liu, G. Xiao, J. Zhu, Z.-K. Zhou, X. Wang, C. Jin, J. Wang, *Nat. Commun.* **2013**, *4*, 2381.

[7] M. Couture, T. Brulé, S. Laing, W. Cui, M. Sarkar, B. Charron, K. Faulds, W. Peng, M. Canva, J.-F. Masson, *Small* **2017**, *13*, 1700908.

[8] M. G. Scullion, A. Di Falco, T. F. Krauss, *Biosens. Bioelectron.* **2011**, *27*, 101.

[9] C. L. Nehl, H. Liao, J. H. Hafner, *Nano Lett.* **2006**, *6*, 683.

[10] I. M. Pryce, Y. A. Kelaita, K. Aydin, H. A. Atwater, *ACS Nano* **2011**, *5*, 8167.

[11] C. Ma, Y. Liu, F. Zhao, F. Xu, J. Yan, X. Li, B.-O. Guan, G. Yang, K. Chen, *J. Mater. Chem. C* **2020**, *8*, 6350.

[12] H. Ni, M. Wang, T. Shen, J. Zhou, *ACS Nano* **2015**, *9*, 1913.

[13] A. Ahmadivand, S. Golmohammadi, *Opt. Laser Technol.* **2015**, *66*, 9.

[14] Y.-L. Liao, Y. Zhao, *Results Phys.* **2020**, *17*, 103072.

[15] Z. Ren, Z. Lin, X. Zhi, M. Li, *Opt. Mater.* **2020**, *99*, 109575.

[16] K. S. Modi, J. Kaur, S. P. Singh, U. Tiwari, R. K. Sinha, *Opt. Commun.* **2020**, 7.

[17] D. U. Yildirim, A. Ghobadi, M. C. Soydan, M. Gokbayrak, A. Toprak, B. Butun, E. Ozbay, *J Phys Chem C* **2019**, 10.

[18] A. J. Ollanik, I. O. Oguntoye, G. Z. Hartfield, M. D. Escarra, *Adv. Mater. Technol.* **2018**, 1800567.

[19] W. Zhang, J. Tu, W. Long, W. Lai, Y. Sheng, T. Guo, *Energy Procedia* **2017**, *130*, 72.

[20] L. Xie, W. Gao, J. Shu, Y. Ying, J. Kono, *Sci. Rep.* **2015**, *5*, 8671.

[21] M. A. Schmidt, D. Y. Lei, L. Wondraczek, V. Nazabal, S. A. Maier, *Nat. Commun.* **2012**, *3*, 1108.

[22] H. Chen, A. M. Bhuiya, R. Liu, D. M. Wasserman, K. C. Toussaint, *J. Phys. Chem. C* **2014**, *118*, 20553.

[23] Y. Yang, I. I. Kravchenko, D. P. Briggs, J. Valentine, *Nat. Commun.* **2014**, *5*, 5753.

[24] M. A. Abbas, A. Zubair, K. Riaz, W. Huang, J. Teng, M. Q. Mehmood, M. Zubair, *Opt. Express* **2020**, *28*, 23509.

[25] M. Askari, M. V. Hosseini, *J. Opt. Soc. Am. B* **2020**, *37*, 2712.

[26] M. D. Allendorf, C. A. Bauer, R. K. Bhakta, R. J. T. Houk, *Chem. Soc. Rev.* **2009**, *38*, 1330.

[27] T. Wagner, S. Haffer, C. Weinberger, D. Klaus, M. Tiemann, *Chem Soc Rev* **2013**, 18.

[28] O. Dalstein, D. R. Ceratti, C. Boissière, D. Grosso, A. Cattoni, M. Faustini, *Adv. Funct. Mater.* **2016**, *26*, 81.

[29] C. Sanchez, C. Boissière, D. Grosso, C. Laberty, L. Nicole, *Chem. Mater.* **2008**, *20*, 682.

[30] D. Grosso, *J. Mater. Chem.* **2011**, *21*, 17033.

[31] T. Bottein, O. Dalstein, M. Putero, A. Cattoni, M. Faustini, M. Abbarchi, D. Grosso, *Nanoscale* **2018**, *10*, 1420.

[32] T. Bottein, T. Wood, T. David, J. B. Claude, L. Favre, I. Berbézier, A. Ronda, M. Abbarchi, D. Grosso, *Adv. Funct. Mater.* **2017**, *27*, 1604924.

[33] M. Bochet-Modaresialam, J.-B. Claude, D. Grosso, M. Abbarchi, *ACS Appl. Nano Mater.* **2020**, *3*, 5231.

[34] M. Boudot, V. Gaud, M. Louarn, M. Selmane, D. Grosso, *Chem. Mater.* **2014**, *26*, 1822.

[35] O. Dalstein, M. Tabo, E. Alvarez, L. Roux, R. Garuz, M. Pasquinelli, L. Azzi, M. Bendahan, K. Aguir, J. Loizillon, M. Abbarchi, D. Grosso, *ACS Appl. Mater. Interfaces* **2019**, *11*, 4439.

Mis en forme : Anglais (États-Unis)